

1      Enhanced blood coagulation and antibacterial activities of carboxymethyl-kappa-carrageenan-  
2      containing nanofibers

3      Liszt Y. C. Madruga<sup>a,b</sup>, Ketul C. Popat<sup>c, d, e</sup>, Rosangela de C. Balaban<sup>a</sup>, Matt J. Kipper<sup>a, c, e</sup>

5      *a – Department of Chemical and Biological Engineering, Colorado State University, Fort Collins, CO. United*  
6      *States*

7      *b – Institute of Chemistry, Federal University of Rio Grande do Norte (UFRN), Natal, RN, Brazil*

8      *c – School of Advanced Materials Discovery, Colorado State University, Fort Collins, CO. United States*

9      *d – Department of Mechanical Engineering, Colorado State University, Fort Collins, CO. United States*

10     *e – School of Biomedical Engineering, Colorado State University, Fort Collins, CO. United States*

12     **ABSTRACT**

13     Ideal wound dressings should be biocompatible, exhibit high antibacterial activity, and promote  
14     blood coagulation. To impart these imperative functions, carboxymethyl-kappa-carrageenan was  
15     incorporated into poly(vinyl alcohol) nanofibers (PVA-CMKC). The antibacterial activity of the nanofibers  
16     was evaluated. Adsorption of two important blood proteins, fibrinogen and albumin, was also assessed. The  
17     adhesion and activation of platelets, and the clotting of whole blood were evaluated to characterize the  
18     ability of the nanofibers to promote hemostasis. Adhesion and morphology of both *Staphylococcus aureus*  
19     and *Pseudomonas aeruginosa* were evaluated using fluorescence microscopy and scanning electron  
20     microscopy. CMKC-containing nanofibers demonstrated significant increases in platelet adhesion and  
21     activation, percentage of coagulation in whole blood clotting test and fibrinogen adsorption, compared to  
22     PVA nanofibers, showing blood coagulation activity. Incorporating CMKC also reduces adhesion and  
23     viability of *S. aureus* and *P. aeruginosa* bacteria after 24 h of incubation. PVA-CMKC nanofibers show  
24     potential application as dressings for wound healing applications.

26     **KEYWORDS**

28     **Keywords:** Carboxymethyl-kappa-carrageenan; Polysaccharides; Platelet adhesion; Protein interaction;  
29     Antibacterial activity; Wound dressings.

31     **1. INTRODUCTION**

32     Skin is an important barrier, providing protection from bacterial infection and environmental  
33     damage (Mogoşanu & Grumezescu, 2014). Skin damage caused by burns, chemicals, and accidents can  
34     lead to wounds with delayed healing and elevated risk of infection. (Dumont et al., 2018). However, wound  
35     healing is a complex sequence involving multiple cell types, which is coordinated by dynamic cytokine

36 signalling. Wound dressings that promote wound healing and prevent infection are an essential resource for  
37 wound treatment.

38 Wound dressings represent a significant component of the healthcare market. (Homaeigohar &  
39 Boccaccini, 2020). Ideal wound dressings should be biocompatible and should support the healing process,  
40 while preventing bacterial infection. Wound dressings should also provide stable coverage, promote  
41 coagulation of the blood to accelerate closure of the wound, absorb wound exudate while maintaining  
42 moisture, and exhibit low adherence to the wound surface, enabling removal without causing additional  
43 trauma (Chattopadhyay & Raines, 2014).

44 Many currently available wound dressings are films, foams, and hydrogels (Almodóvar et al., 2013;  
45 Bajpai & Daheriya, 2014; da Cruz et al., 2020; Das et al., 2019; Fujiwara et al., 2012; Yegappan et al.,  
46 2018; Zia et al., 2017). Nanofibrous materials have emerged as new wound dressings, due to their notably  
47 large exposed surface area and nanoporosity, normally on the scale of nanometers. These characteristics  
48 can mimic the extracellular matrix (ECM) structure, facilitating interactions with cells in the wound bed  
49 (Bhattacharjee et al., 2020; Guo et al., 2016; Sadeghi et al., 2019; Truong et al., 2012; Unnithan et al., 2015;  
50 Xu et al., 2015). Electrospinning is a well-established technique for the production of nanoscale fibers.  
51 Electrospun nanofibers comprise highly porous 3D structures, that enhance cell-material and cell-cell  
52 interactions, while maintaining or enhancing the biological properties of the material used for nanofiber  
53 preparation. Moreover, the simplicity and low operating cost make electrospinning a compelling method  
54 for production of nanostructured materials (Madruga et al., 2021; Mogoșanu & Grumezescu, 2014).  
55 Electrospun nanofibers can be modified to incorporate biological signals that promote healing. However,  
56 incorporation of all functions necessary to promote wound healing into synthetic polymers increases the  
57 complexity and cost of the process, reducing manufacturability. On the other hand, natural polymers with  
58 inherent biocompatibility and biological activities, combined with the favorable wound healing properties  
59 introduced via electrospinning can overcome many of these challenges (de Oliveira et al., 2021; do  
60 Nascimento Marques et al., 2020; Miguel et al., 2018; Zahedi et al., 2010; R. Zhao et al., 2014).

61 Nanofibers can be prepared from natural polymers that possess similar chemical compositions to  
62 components of the extracellular matrix, facilitating the manufacture of fibers similar to the ECM (Young  
63 et al., 2017). Nanofiber-based dressings for wound healing should possess favorable biological properties,  
64 including cytocompatibility, moisture retention, blood coagulant activity, antibacterial activity, non-  
65 toxicity, and low cost (Abrigo et al., 2014; Fahimirad & Ajalloueian, 2019; Felgueiras & Amorim, 2017;  
66 Haider et al., 2018; Trinca et al., 2017; Zia et al., 2017).

67 Carrageenan and derivatives of carrageenan are attractive biomaterials. Carrageenans are sulfated  
68 polysaccharides, affording the opportunity to introduce biochemical functionality of sulfated polymers,  
69 without requiring harsh and hazardous sulfation/sulfonation chemistries. Previous work from our labs has  
70 shown that carboxymethyl kappa-carrageenan (CMKC) exhibits high cell viability, no cytotoxicity toward  
71 human adipose-derived stem cells (ADSCs), and no hemolytic activity toward human red blood cells.  
72 Furthermore, these materials exhibit increased antioxidant activity and they inhibit *Staphylococcus aureus*,  
73 *Bacillus cereus*, *Escherichia coli*, and *Pseudomonas aeruginosa* (Madruga et al., 2020).

74 Electrospinning of CMKC is difficult because it is a strong polyelectrolyte. Therefore, we blended  
75 CMKC with poly(vinyl alcohol) (PVA) to form PVA-CMKC aqueous solutions, to improve the spinnability  
76 of CMKC, and successfully produced nanofibers. Both PVA and CMKC are hydrophilic, making the  
77 electrospun fibers water soluble as well, and therefore unsuitable for wound dressing applications, since  
78 they need to be able to absorb the exudate of the wounds. Thermal crosslinking for 8 h at 180 °C induces  
79 ester bond formation between carboxyl groups in CMKC and hydroxyl groups in PVA making them  
80 insoluble in water (Madruga et al., 2021). The CMKC-containing nanofibers exhibit high cytocompatibility,  
81 cell growth and cell adhesion of ADSCs, biodegradability in a lysozyme solution, and enhanced ADSC  
82 response with respect to osteogenic differentiation (Madruga et al., 2021). These properties suggest that  
83 CMKC-containing nanofibers are excellent candidate biomaterials for tissue engineering. However, the  
84 hemostatic property and antibacterial activity of these nanofibers, which are important properties for wound  
85 healing, have not been reported.

86       Based on our previous work, we hypothesize that antimicrobial activity and procoagulant activity  
87    can be introduced into nanofibers by blending CMKC with PVA. In this work, we evaluated the  
88    antibacterial activity and blood protein interactions with PVA-CMKC electrospun nanofibers (0, 25, 50 and  
89    75% wt. CMKC). In this work, the nanofibers were exposed to protein solutions (fibrinogen and albumin),  
90    platelet-rich plasma (PRP), human whole blood, and bacteria inocula. Protein adsorption was evaluated by  
91    X-ray photoelectron spectroscopy (XPS). The amount of adhered platelets and blood clotting index were  
92    analysed by, scanning electron microscopy (SEM), fluorescence microscope images and absorbance  
93    measures. The adhesion and cellular integrity of *S. aureus* and *P. aeruginosa* on the nanofibers were  
94    evaluated by SEM images and fluorescence microscope images using live/dead staining. PVA-CMKC  
95    nanofibers may have improved features and functions compared to other wound dressing formulations (e.g.,  
96    hydrogels), such as increased surface area, nanoscale topographic features, the ability to absorb the exudate  
97    of the wounds, hemostatic activity, and antibacterial activity. PVA-CMKC nanofibers may therefore be  
98    used as dressings for wound healing applications.

## 99    **2. EXPERIMENTAL SECTION**

### 100   **2.1. Materials**

101       Poly(vinyl alcohol) 87–89% hydrolyzed (PVA) of  $M_w$   $1.46\text{--}1.86 \times 10^5$  g mol $^{-1}$ , kappa-carrageenan  
102    (KC) of  $M_w$   $3.9 \times 10^5$  g mol $^{-1}$  [determined previously by our group (Madruga et al., 2018)] and  
103    monochloroacetic acid (MCA) were purchased from Sigma-Aldrich (USA). LB broth (Miller) was  
104    purchased from Fisher (USA). Millipore water was used in the preparation of all aqueous solutions.

### 105   **2.2. Carboxymethylation of kappa-carrageenan**

106       Williamson's ether synthesis procedure was followed to carboxymethylate KC, according to  
107    previous protocols (Madruga et al., 2020, 2021). Briefly, KC (10 g) was suspended in an aqueous solution  
108    (200 mL) containing 80% (w/v) of 2-propanol in a three-necked glass flask coupled with a reflux condenser.  
109    A 20% (w/v) NaOH aqueous solution (20 mL) was added dropwise over 15 min. The reaction mixture was

110 kept at 40 °C for 1 h with vigorous stirring. A solution of monochloroacetic acid (8.75 g in 20 mL of 20%  
111 NaOH aqueous solution) was added dropwise with a syringe over 20 min to the KC solution, and the  
112 temperature was maintained at 55 °C for 4 h with stirring. The product was recovered through vacuum  
113 filtration and washed three times with 80% 2-propanol aqueous solution and pure 2-propanol. The  
114 precipitate was dissolved in deionized water (300 mL) overnight. The solution was dialyzed against water  
115 through a membrane (7000 Da maximum molecular weight cutoff) until the conductivity was below 20  
116 mS.cm<sup>-1</sup>, measured with a conductivity meter from Thermo Orion, model Orion 145A+, with conductivity  
117 cell Orion 011510 (USA). Finally, the material was freeze-dried in a ModulyoD lyophilizer from  
118 ThermoSavant. The reaction was conducted with the molar ratio of MCA:KC monomer of 3.5:1, yielding  
119 CMKC with a degree of substitution (DS) of 1.1 ( $M_w 4.3 \times 10^5$  g mol<sup>-1</sup>). This DS was chosen based on our  
120 previous evaluation of different CMKC DS and biological assays (Madruga et al., 2020, 2021). The  
121 modified KC is referred to as carboxymethyl-kappa-carrageenan (CMKC).

122 **2.3. Electrospinning of PVA-CMKC nanofibers**

123 Nanofibers were fabricated by electrospinning following procedures from our previous report  
124 (Madruga et al., 2021). Briefly, the solutions were prepared by blending PVA and CMKC at different  
125 weight ratios in water (5.0 mL) and stirring overnight. The CMKC content (wt.%) is reported relative to  
126 the total polymer concentration (which is 5% w/v for all samples) in the final solution. Four compositions  
127 were used in this study, with 0, 25, 50 and 75 wt. % CMKC. The blend solutions were pumped (at 1.0 mL  
128 h<sup>-1</sup> for 5 hours), using a syringe pump (Genie Plus, Kent Scientific, Torrington, CT), through a 19-gauge  
129 needle (1.07 mm diameter). Electrospinning was carried out at ambient conditions (19 ± 1 °C and 18%  
130 relative humidity), at a field strength of 1 kV cm<sup>-1</sup> provided by a DC power supply (Gama High Voltage  
131 Research, Ormond Beach, FL). Nanofibers were collected on aluminum foil on a copper plate. The nozzle-  
132 to-collector distance was set as 15 cm. The nanofibers were cut into 8-mm diameter circles for all  
133 subsequent assays. For crosslinking, heat treatment of the nanofibers in a vacuum oven at 180 °C for 10 h  
134 was performed (Madruga et al., 2021).

135 **2.4. Characterization of PVA-CMKC nanofibers**

136 Nanofiber chemical composition was characterized by X-ray photoelectron spectroscopy (XPS)  
137 (5800 spectrometer, Physical Electronics, Chanhassen, MN) using. Survey spectra were collected from 0  
138 to 1100 eV, with a pass energy of 187 eV. The C1s peak (284.8 eV) was used as reference. High-resolution  
139 spectra of the C1s envelopes were also acquired with 0.1 eV steps and an X-ray spot of 800  $\mu\text{m}$ . Origin and  
140 Multipak Software were used for performing the curve fitting of all presented spectra.

141 **2.5. Hemostatic activity**

142 *2.5.1. Protein adsorption on the nanofibers*

143 The adsorption of fibrinogen (FIB) and albumin (ALB) to nanofibers was investigated following  
144 the procedure reported on literature (da Câmara et al., 2020; Sabino et al., 2020; Sabino et al., 2019). The  
145 nanofibers were sterilized by immersion in 70% ethanol for 15 min and washed 3 times with sterile  
146 phosphate-buffered saline (PBS). Sterilized nanofibers were incubated in a 48-well plate with 100  $\mu\text{g mL}^{-1}$   
147 solution of human fibrinogen or albumin at 37 °C for 2 h with 100 rpm shaking. All samples were rinsed  
148 with PBS and water before analysis. The surface composition of adsorbed samples before and after protein  
149 adsorption was characterized by the C1s envelope using high-resolution XPS spectra, by evaluating the C–  
150 N peaks.

151 *2.5.2. Platelet adhesion and activation*

152 For this study two healthy individuals consented to donate blood via venous phlebotomy, using  
153 procedures approved by the Colorado State University Institutional Review Board, in accordance with the  
154 National Institutes of Health’s “Guiding Principles for Ethical Research.” Blood was drawn by a  
155 phlebotomist (into 10 ml EDTA-coated vacuum tubes). Whole blood was centrifuged (100 $\times\text{g}$  for 15 min).  
156 The plasma containing the platelets and leukocytes was removed and allowed to rest for 10 min before use,  
157 to obtain platelet-rich plasma (PRP). Fluorescence microscopy was used to evaluate the platelet adhesion  
158 on the nanofibers (da Câmara et al., 2020; Sabino et al., 2020). Six separate samples of each nanofiber were

159 used for fluorescence microscopy. Each sample was placed in the well of a 48-well plate and incubated  
160 with 500  $\mu$ L of PRP (37 °C for 2 h with 100 rpm shaking). Following incubation with PRP, samples were  
161 rinsed with PBS and water before analysis, to remove non-adhered platelets. The samples were then stained  
162 with calcein-AM live stain (Invitrogen) solution in (2  $\mu$ M, in PBS) for 30 min with 100 rpm shaking at  
163 room temperature, protected from light. The samples were imaged using a Zeiss Axiovision fluorescence  
164 microscope using a 493/514 nm filter and five images from randomly selected locations were taken from  
165 each of three samples per condition. ImageJ software was used to calculate the percentage of the area with  
166 adhered platelets.

167 Platelet activation was also characterized by scanning electron microscopy (SEM) on three separate  
168 samples of each nanofibers. The nanofibers were incubated for 2h in PRP, then rinsed twice with PBS and  
169 were fixed with primary fixative (3.0% glutaraldehyde, 0.1 M sodium cacodylate, and 0.1 M sucrose) for  
170 45 min. Primary fixation was followed by a 10-min secondary fixation (using primary fixative without  
171 glutaraldehyde). After fixation, the nanofibers were dehydrated with consecutive solutions of ethanol (35,  
172 50, 70, and 100%, respectively) for 10 min each. All samples were sputter-coated with gold (15 nm) and  
173 imaged via SEM (JSM-6500F JEOL, Tokyo, Japan) using an accelerating voltage of 15 kV. Five images  
174 of randomly selected locations were taken from each of three samples per condition. The SEM images  
175 were used to visualize platelet adhesion and morphology, indicative of platelet activation.

176 *2.5.3. Whole blood clotting*

177 Human blood from healthy donors was drawn into 3 ml vacuum tubes with no anticoagulants by a  
178 trained phlebotomist. To evaluate whole blood clotting kinetics, sterilized nanofiber samples were placed  
179 in a 24-well plate and 5.0  $\mu$ L of whole blood was dropped on each sample and allowed to clot for 15 and  
180 30 min. In a different 24-well plate, with 500  $\mu$ L DI water, the nanofibers were gently agitated for 5 min  
181 on a shaker to lyse the red blood cells and release free hemoglobin. The absorbance of free hemoglobin was  
182 measured using a plate reader (Molecular Devices Spectra Max M3) at 540 nm. The control for 100% free

183 hemoglobin was obtained from a sample solubilized in water and measured immediately after collection (0  
184 min) (da Câmara et al., 2020; Sabino & Popat, 2020).

185 **2.6. Antibacterial activity**

186 A standardized inoculum of each strain (*Pseudomonas aeruginosa* P01 and *Staphylococcus aureus*  
187 ATCC 6538) was prepared by suspending colonies directly in a nutrient broth media solution (LB-Miller -  
188 25 mg mL<sup>-1</sup>) diluted to obtain a concentration of 10<sup>6</sup> CFU/mL. To evaluate the antibacterial activity, 500  
189 µL of bacteria solution were added to the sterilized nanofibers for 6 and 24 h.

190 *2.6.1. Bacteria adhesion and morphology on the nanofibers*

191 The adhesion of live and dead bacteria adhered on the nanofibers was evaluated using a live/dead  
192 stain (3 µL/mL of propidium iodide and Syto 9 stain 1:1 in PBS), following the protocol of the  
193 manufacturer, and quantified from fluorescence microscope images. The nanofibers were rinsed with PBS  
194 three times after the incubation period, and the stain solution was added and allowed to react with the  
195 samples for 20 minutes. Then the nanofibers were rinsed with PBS and imaged on a Zeiss Axiovision  
196 fluorescence microscope. The percentage of live and dead bacteria on the nanofibers was determined by  
197 analyzing the fluorescence microscopy images in ImageJ. Five images from randomly selected locations  
198 were taken from each of three samples per condition.

199 Scanning electron microscopy was used to investigate the morphology of the adhered bacteria and  
200 biofilm formation on the nanofibers. After incubation for 6 and 24 h in bacteria broth, the nanofibers were  
201 rinsed with PBS to remove non-adhered bacteria. The samples were fixed and dehydrated as described  
202 above for the platelet SEM images (section 2.5.2).

203 **2.7. Statistical analysis**

204 At least three different samples of each nanofiber type were used in all experiments; results are  
205 presented as mean  $\pm$  standard deviation. Differences were determined using one-way ANOVA ( $p = 0.05$ )  
206 with a post-hoc Tukey's honest significant difference test.

207 **3. RESULTS AND DISCUSSION**

208 **3.1. Characterization of PVA/CMKC Nanofibers**

209 The SEM images agree with the fiber morphology of our previous study, showing that the thermal  
210 crosslinking maintains the morphology of all nanofibers and makes them insoluble in water (Figure S1 in  
211 the supplementary information).

212 XPS data confirm the chemical composition of the crosslinked nanofibers. Survey spectra of the  
213 nanofibers have oxygen (O1s) and carbon (C1s) peaks, and CMKC-PVA nanofiber spectra also have sulfur  
214 (S2s and S2p) peaks, from the sulfate groups in CMKC (Figure S2 – supplementary information). From  
215 survey XPS scans, elemental composition of the nanofibers was obtained, and the data are shown in **Table**  
216 **1**. The CMKC-containing nanofibers have increasing sulfur content with increasing concentration of  
217 CMKC on the samples. High-resolution XPS C1s spectra were also collected (**Figure 1a**). The CMKC-  
218 containing nanofibers have a significant increase in –COOH groups, compared to the PVA nanofibers, due  
219 to the presence of the carboxymethyl group on CMKC. The crosslinked nanofibers contain ether and ester  
220 bonds resulting in peaks in the region of 286 eV and overlap with the bonds C–OH. However, previously  
221 reported infrared spectra confirmed the presence of the crosslinked sites with peaks between 1700 and 1750  
222  $\text{cm}^{-1}$  (Madruga et al., 2021). The incorporation of CMKC is therefore confirmed by the XPS spectra and  
223 agrees with the FTIR data from our previous study.

224

225 **Table 1.** Elemental composition of the nanofibers.

	% C1s	% N1s	% O1s	% S2p
<b>PVA</b>	70.53	0.00	29.47	0.00
<b>PVA-CMKC 25%</b>	66.78	0.00	32.79	0.43
<b>PVA-CMKC 50%</b>	60.99	0.00	38.50	0.51
<b>PVA-CMKC 75%</b>	65.15	0.00	34.18	0.67

226

227 **3.2. Hemostatic activity**228 *3.2.1. Protein adsorption on the nanofibers*

229 Blood clot formation results from the activation and aggregation of platelets, and a multistep  
 230 coagulation cascade, culminating with the polymerization of fibrinogen and formation of a network of  
 231 crosslinked fibrin fibers (Hedayati et al., 2019). The monolayer of proteins that adsorbs on the surface of a  
 232 biomaterial is a mediator to the formation of a clot, and its composition can dictate subsequent biological  
 233 protein processes (Prawel et al., 2014). Albumin (ALB) is one of the most abundant proteins in the blood.  
 234 Albumin adsorption can block or promote coagulation, depending on whether it is in its native conformation  
 235 or denatured (Paar et al., 2017). Fibrinogen (FIB) is spindle or rod-shaped protein that is converted to the  
 236 polymerizable form, fibrin, in the blood coagulation cascade. As the precursor of the polymerizable fibrin,  
 237 FIB is essential for the formation of blood clots and provides binding sites for platelets (da Câmara et al.,  
 238 2020; Sabino et al., 2019).

239 High-resolution XPS spectra of the C1s envelope and survey spectra were obtained for the  
 240 nanofibers after incubation in human albumin and fibrinogen solutions. The amount of proteins adsorbed  
 241 to the nanofibers was estimated by the elemental composition. Since the nanofibers have no nitrogen in  
 242 their structure (**Table 1**), the increase in nitrogen elemental composition obtained from the XPS survey  
 243 scans on the fibers is evidence of protein adsorption (**Table 2**). The adsorption of FIB and ALB on the  
 244 fibers was evaluated from the high-resolution spectra for the C1s envelope by analysing the increment of  
 245 the amide carbonyl (N–C=O) peaks (**Figure 1b**).

246 **Table 2.** Nitrogen content in the surface of the nanofibers before and after protein adsorption  
 247 experiments, obtained from XPS survey scans.

	% N (before)	% N (fibrinogen)	% N (albumin)
<b>PVA</b>	0.00	5.28	3.03
<b>PVA-CMKC 25%</b>	0.00	3.38	1.83
<b>PVA-CMKC 50%</b>	0.00	4.69	0.17
<b>PVA-CMKC 75%</b>	0.00	3.13	0.61

248

249 FIB promotes platelet adhesion and activation, by exposing binding sites to platelets and allowing  
 250 the clotting formation. Thus, an increase in the adsorption of fibrinogen on the nanofibers can be correlated  
 251 with increasing pro-coagulant capacity. ALB, on the other hand, can block or promote the formation of  
 252 clots, depending on the conformation adopted or denaturation. The high-resolution XPS spectra of the C1s  
 253 envelope (**Figure 1b**) shows similar amide peak (N–C=O) increases following adsorption of both proteins  
 254 to PVA nanofibers. PVA-CMKC nanofibers all exhibit larger nitrogen content increases following  
 255 fibrinogen adsorption compared to albumin adsorption. PVA nanofibers have the highest nitrogen content  
 256 following both FIB and ALB adsorption. The same trend is observed when comparing the amide peak in  
 257 the C1s spectra for both the PVA-CMKC 25% and 75% (**Figure 1b**). This suggests that adding CMKC to  
 258 nanofibers may promote higher coagulation and blood clot formation, due to higher protein adsorption.  
 259 Even after crosslinking, all nanofibers still present some hydrophilicity, however, the nanofibers containing  
 260 CMKC present more crosslinking sites, due to presence of the carboxymethyl groups, which make them a  
 261 little more hydrophobic when compared to pure PVA. The pure PVA nanofibers had the highest amount of  
 262 proteins adsorbed, which can be associated to the high surface area of this fiber and due to the hydroxyl  
 263 and ester groups that can promote protein adsorption and changes in protein conformation (Sivaraman &  
 264 Latour, 2010; Yang et al., 2017). The high adsorption of albumin in PVA nanofibers might block platelet  
 265 adhesion decreasing clot formation, and the hydrophilicity can lead to a decrease of the platelet binding  
 266 sites of the fibrinogen adsorbed (Zhang et al., 2017). On the other hand, increasing the concentration of  
 267 CMKC on the nanofibers up to 50% decreases the albumin adsorption and increases the fibrinogen

268 adsorption, which promotes more sites for platelets to bind and form clots. The chemical similarity of  
269 CMKC to biological molecules, such as glycosaminoglycans, found in the human body as well as the large  
270 number of hydrogen-bonding groups present on the molecule may promote protein-material interactions  
271 (Rodrigues et al., 2006). The PVA-CMKC 75% nanofibers had less fibrinogen and more albumin adsorbed  
272 when compared to the PVA-CMKC-50% nanofibers, which could lead to reduced platelet adhesion and  
273 activation. The smaller amount of proteins adsorbed can be correlated to the higher dispersity in the fiber  
274 diameter, due to the higher instability when electrospinning a high charge-density solutions (Haider et al.,  
275 2018; Merkle et al., 2015a).

276

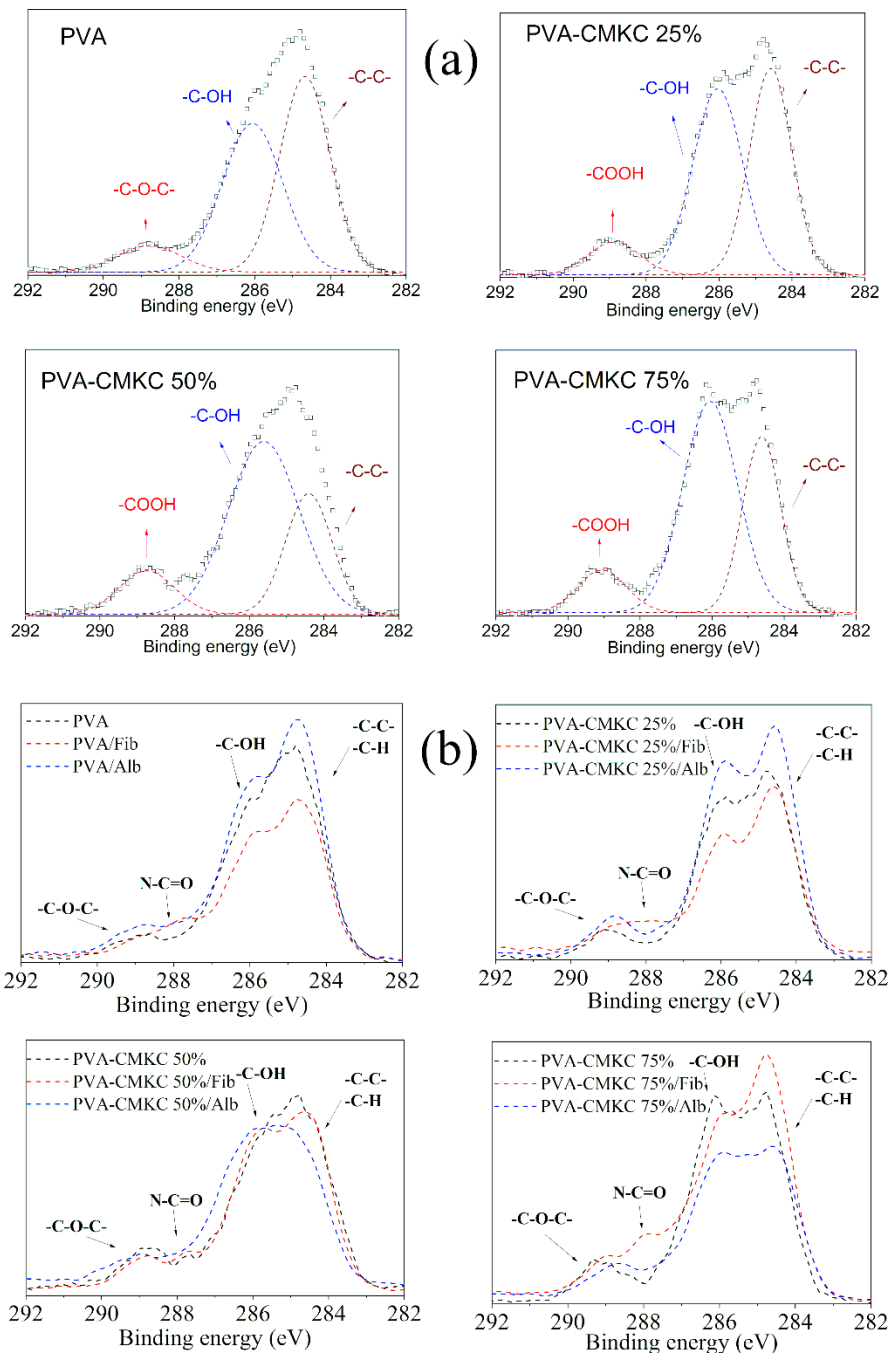
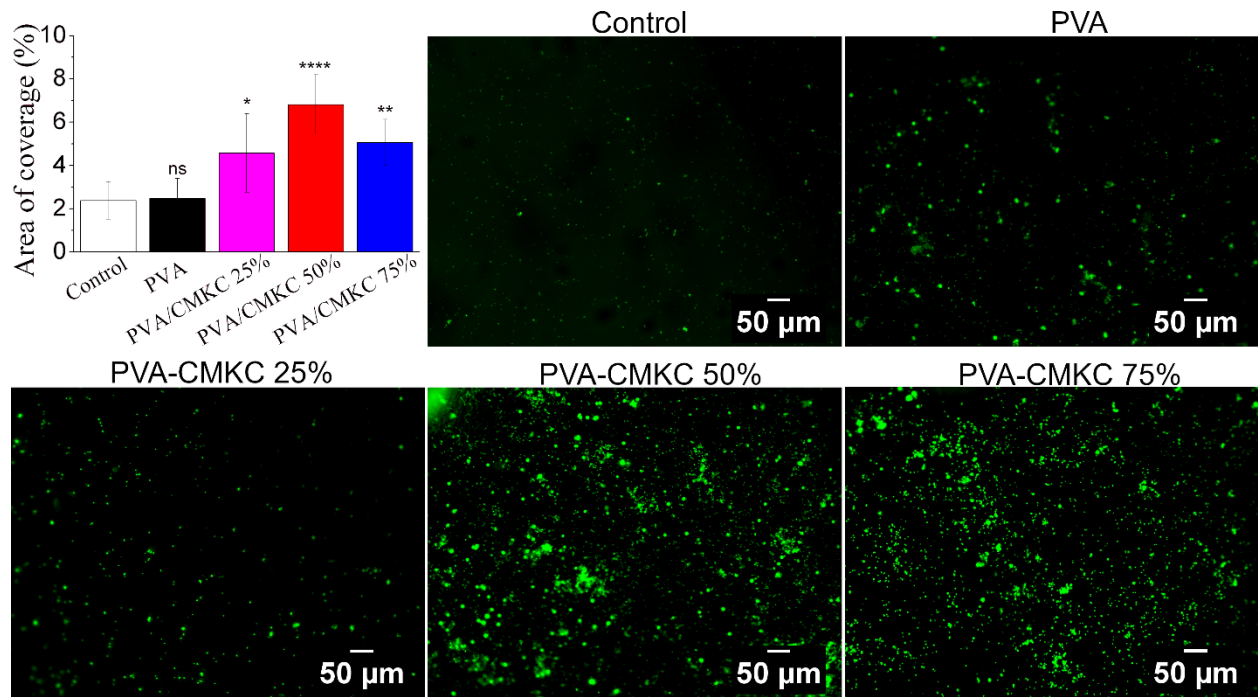


**Figure 1.** XPS high-resolution C1s spectra for crosslinked nanofibers (a); High-resolution C1s spectra for FIB and ALB adsorbed on nanofibers showing C–H, C–C, C–OH, N–C=O and C–O–C signals (b).

282 Platelet adhesion on the surfaces of biomaterials is an indicator of thrombogenicity and pro-  
283 coagulant activity, leading to platelet activation, which can initiate the coagulation cascade (Hedayati et al.,  
284 2019). **Figure 2** illustrates the adhesion of platelets (green) on the surface of the nanofibers and tissue  
285 culture polystyrene (control) following 2 h incubation in human PRP. Nanofibers exhibit a significant  
286 increase in platelet adhesion compared to the control, which increases with increasing CMKC content. The  
287 difference in the number of adhered platelets between the fibers and the control can be attributed partially  
288 to the relatively high specific surface area and nanoscale topography of the nanofibers compared to the two-  
289 dimensional control surface. Because they have a three-dimensional structure and a rough surface with  
290 pores, nanofibers tend to have a higher deposition of platelets and proteins on their surface (Zeng et al.,  
291 2016). Moreover, when compared with PVA nanofibers, CMKC-containing nanofibers also have higher  
292 platelet adhesion (**Figure 2**). This suggests that CMKC enhances platelet adhesion. The formation of ester  
293 groups by crosslinking with PVA may also contribute to increased platelet adhesion (Ma et al., 2015;  
294 Madruga et al., 2020).

295 Platelet adhesion to surfaces can lead to rapid platelet activation. Activated platelets undergo a  
296 series of morphological changes, including spreading, dendrite formation and then aggregation (da Câmara  
297 et al., 2020; Sabino et al., 2019). While non-activated platelets are spherical, platelets undergoing activation  
298 exhibit long, finger-like extensions. Fully activated platelets are characterized as having a “fried egg”  
299 appearance (Simon-Walker et al., 2017; Vlcek et al., 2021). The morphology of the platelets adhered on  
300 the nanofibers was evaluated by SEM images (**Figure 3**). The high number of adhered platelets on the  
301 CMKC-containing nanofibers seen in the SEM images confirms the observations in the fluorescence  
302 micrographs, demonstrating that CMKC promotes platelet adhesion. All platelets show dendrite formation  
303 and a very small number are in a round (unactivated) morphology. Heparin, another sulphated  
304 polysaccharide can have anticoagulant activity, through interactions with antithrombin III and other  
305 components of the coagulation cascade. Nonetheless, when adsorbed to a surface heparin can also promote  
306 platelet activation on nanostructured surfaces, as its negatively charged sulfate groups form complexes with

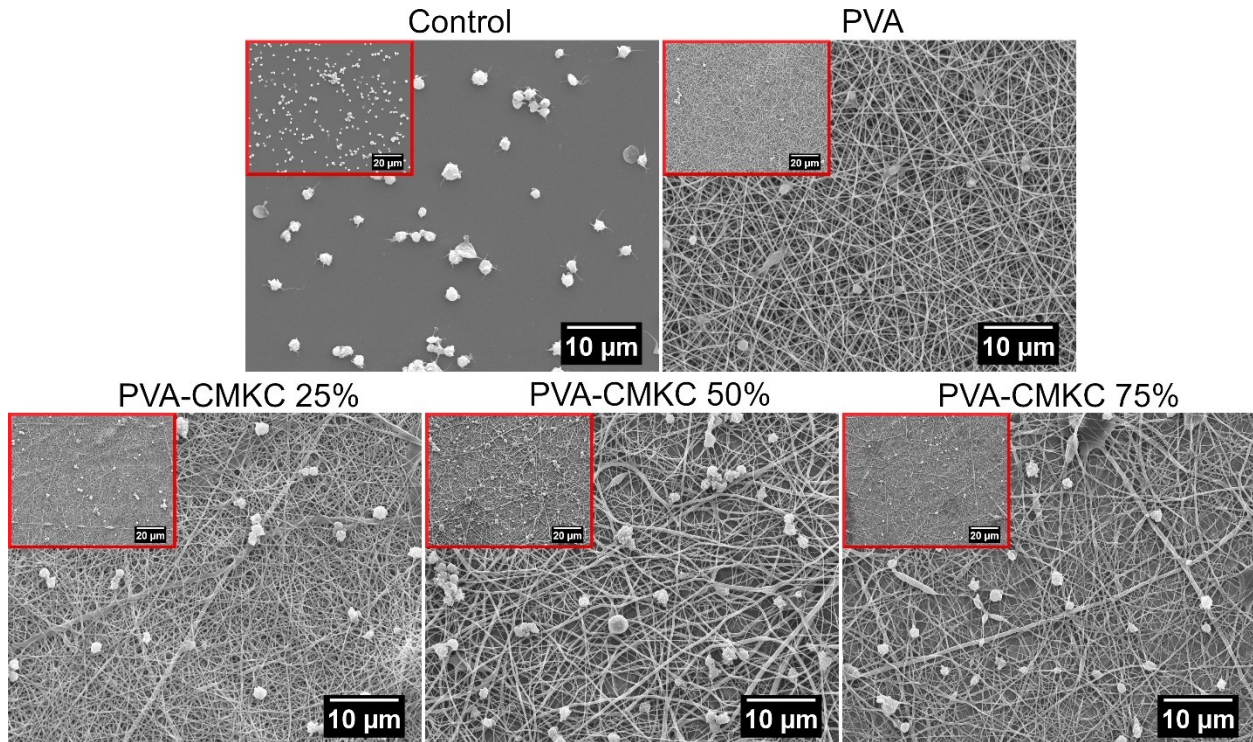
307 positively charged platelet factor 4, which can result in immune complexes that activate platelets (Krauel  
308 et al., 2012; Vlcek et al., 2021).



309  
310 **Figure 2.** Percentage area of adhered platelets on nanofibers, and fluorescence microscopy images of  
311 adhered platelets stained with calcein-AM on the nanofibers after 2 h of incubation in platelet-rich  
312 plasma. CMKC-containing nanofibers have significantly higher platelet adhesion compared to control.  
313 \*\*\*\*  $p \leq 0.0001$ , \*\*  $p \leq 0.01$ , \*  $p \leq 0.05$  and “ns”  $p \geq 0.05$ .  
314

315 Platelets have negatively charged membranes. Since the CMKC is also negatively charged,  
316 electrostatic forces alone would cause CMKC to repel platelets from the nanofibers. However, this is not  
317 what is observed from the results on Figure 2. In fact, studies have shown that carboxyl groups, which are  
318 also present in CMKC, have relatively little impact on platelet adhesion and aggregation (Dorahy et al.,  
319 1997; Wilner et al., 1968). However, studies have shown that a negatively charged surfaces can activate  
320 factor XII and platelet factor 3, leading to intrinsic blood coagulation (Tranquilan-Aranilla et al., 2016).  
321 We suggest that the processes that lead to platelet adhesion and activation on CMKC-containing nanofibers  
322 are related to attachment of plasma proteins and interactions of the platelets with these proteins attached to  
323 the nanofibers (Rodrigues et al., 2006). Since this work used PRP, all the proteins present on the plasma

324 (such as fibrinogen and complement proteins) can attach to the nanofibers and provide sites for the platelets  
325 to interact and attach. The presence of fibrinogen on the nanofibers shown on Figure 1 and Table 2  
326 corroborates these results. Data from the literature shows that fibrinogen adsorption is related to high  
327 platelet adhesion and activation and the conformation of the protein is relevant to this mechanism  
328 (Chiumiento et al., 2007; Rodrigues et al., 2006). Zhang et al (2017) observed that on hydrophilic surfaces  
329 the  $\gamma$ 400-411 platelet-binding dodecapeptide on the D region of fibrinogen is exposed, leading to formation  
330 of uniform monolayers of activated platelets on the surface (Zhang et al., 2017). Similar phenomena could  
331 be responsible for the observed platelet activation on the CMKC nanofibers reported here. In addition, the  
332 similarity of CMKC to biological molecules can promote biochemical signals and sites for the deposition  
333 and activation of platelets (Merkle et al., 2015b). Increasing the amount of CMKC to 75% made the fibers  
334 more unstable, due to the high presence of charges in solution when electrospinning, resulting in the highest  
335 fiber roughness and fiber porosity, and perhaps lower surface area for protein adsorption and subsequent  
336 platelet adhesion. This explains why the nanofibers with 75% CMKC presented lower number of platelets  
337 adhered, when compared to the ones with 50% CMKC. This trend also correlates to the higher amount of  
338 albumin and lower amount of fibrinogen on the 75% CMKC samples, compared to the 50% CMKC  
339 samples. Nonetheless, the difference in area of adhered platelets between the 50% and 75% CMKC  
340 nanofibers is not statistically significant.



341

342 **Figure 3.** SEM micrographs of adhered platelets on the nanofibers after 2 h of incubation in platelet-rich  
 343 plasma.  
 344

345 *3.2.3. Whole blood clotting*

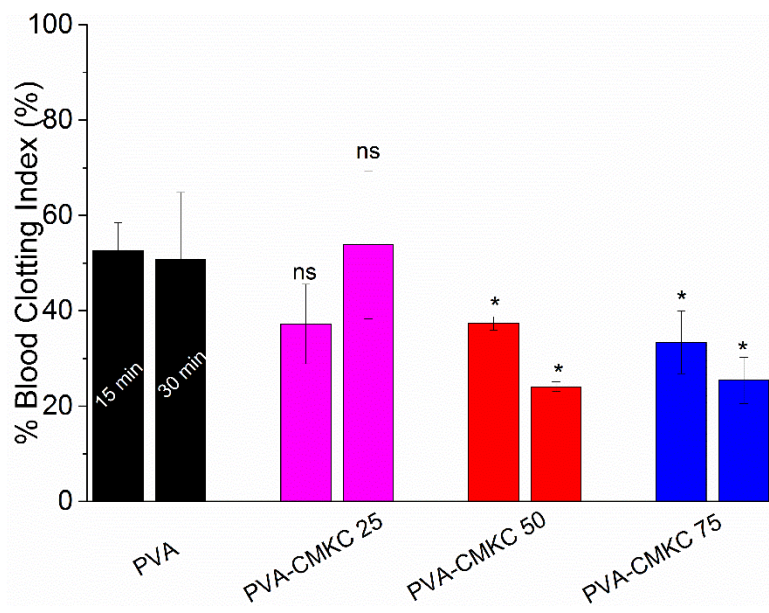
346 Blood clotting tests using human blood (plasma and erythrocytes) characterize the biochemical  
 347 reactions involved in the hemostatic response. Although the investigation of single components of the  
 348 coagulation cascade can provide information on specific interactions between blood components and the  
 349 biomaterial, whole blood clotting offers the most accurate and clinically relevant thrombogenicity index,  
 350 presenting the combined effects of all components (Sabino & Popat, 2020).

351 Human blood droplets were applied to the nanofibers and the clot formation after 15 and 30 min  
 352 were analysed by absorbance measurements of the samples for the free hemoglobin released from the un-  
 353 clotted blood (**Figure 4**). The blood clotting index (BCI) was calculated for all samples and the values of a  
 354 blood sample in water at time 0 (as soon as the blood is collected) (Barba et al., 2018; X. Zhao et al., 2018).  
 355 Absorbance measurements were scaled from 0% to 100% free hemoglobin. Accordingly, the absorbance

356 values the percentage of free hemoglobin for each sample were calculated and reported as blood clotting  
357 index, as shown in **Figure 4**. A reduction in the free hemoglobin indicates an increase in the procoagulant  
358 activity. These results agree with the results from serum protein adsorption and from platelet adhesion and  
359 activation. All nanofiber samples exhibit some non-zero pro-coagulation activity; nanofibers with higher  
360 CMKC content (50 and 75%) resulted in significantly lower BCI than PVA nanofibers, reaching values  
361 close to 20%, with no statistically significant difference between the two. Therefore both the nanoscale  
362 features of the fibers and their chemistry promote coagulation (Vögtle et al., 2019; Xu et al., 2015). The  
363 hemostatic effects of CMKC hydrogels are similar to the ones observed in CMKC nanofibers in terms of  
364 BCI and platelet adhesion, confirming the contribution of CMKC to the hemostatic behavior (Tranquillan-  
365 Aranilla et al., 2016). CMKC-containing nanofibers with greater than 50% CMKC are strong candidates  
366 for application in wound dressings based on the observed pro-coagulant activity.

367

368



369

370 **Figure 4.** Whole blood clotting measured by the normalized amount of free hemoglobin in human whole  
371 blood incubated with nanofibers for 15 and 30 min. Reduced blood clotting index indicates increased  
372 clotting. \*  $p \leq 0.05$  and “ns”  $p \geq 0.05$  compared to the PVA control.

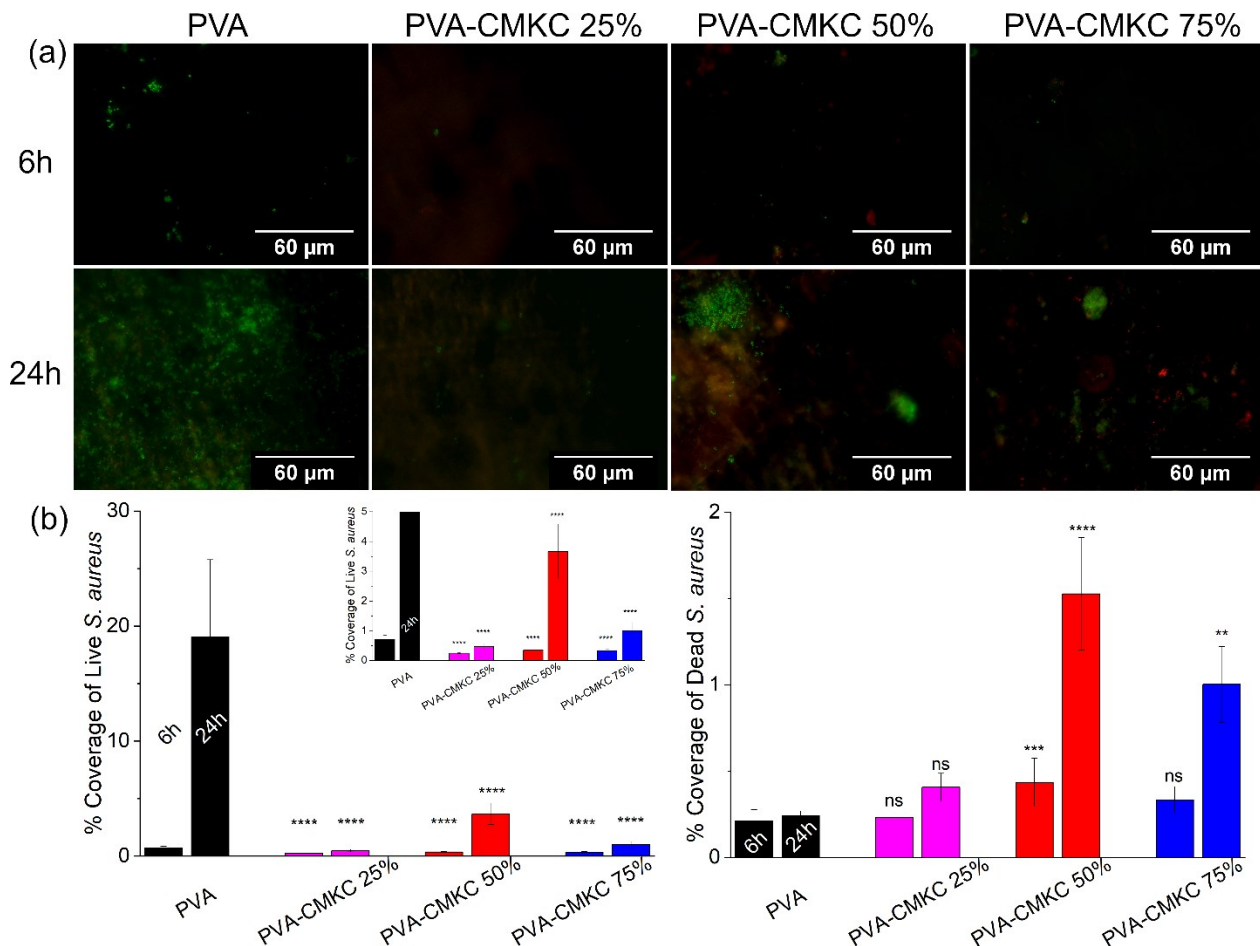
373

374 **3.3. Antibacterial activity**

375 *3.3.1. Bacteria adhesion on the nanofibers*

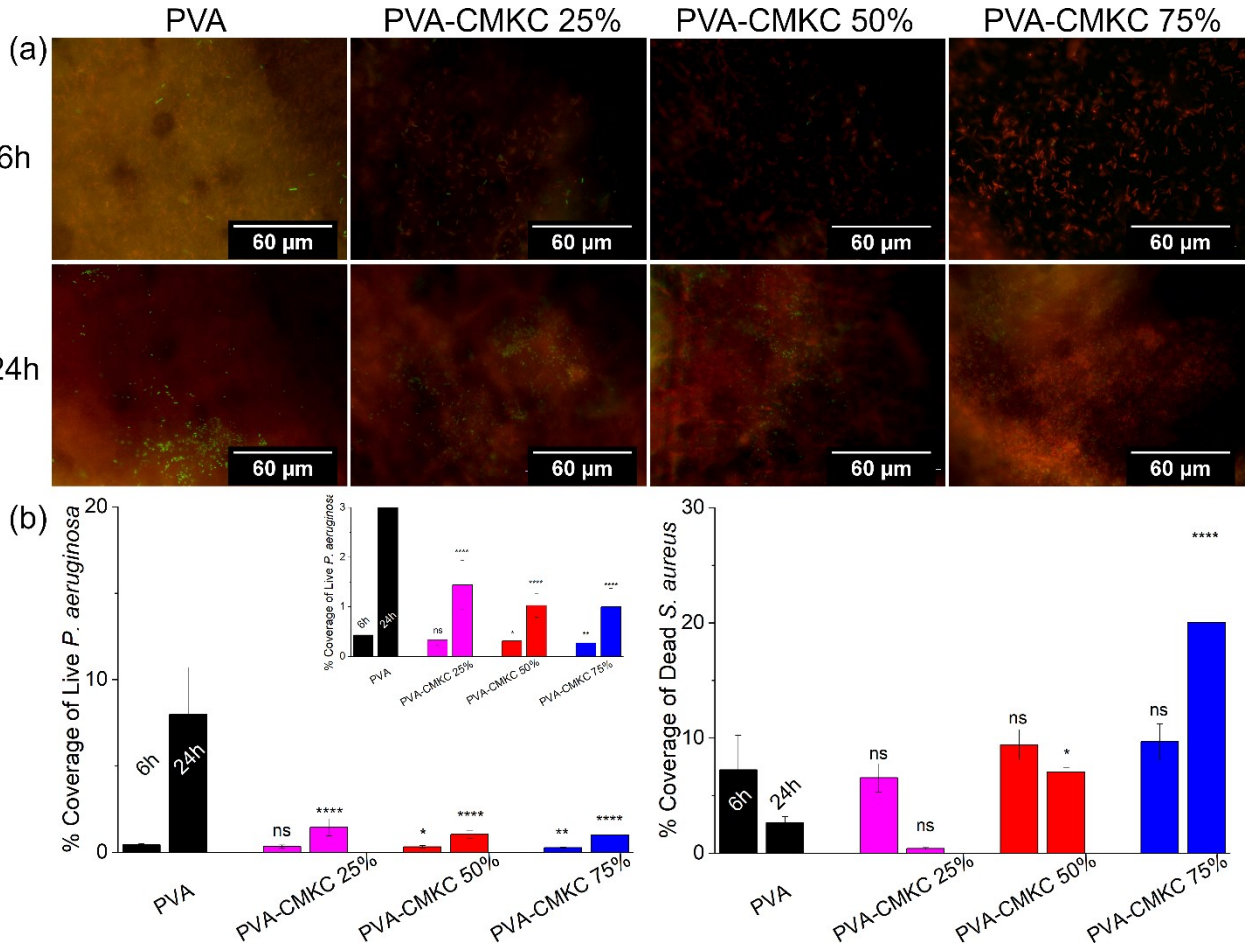
376 Exposed wounds are viable environments for the colonization of bacteria, especially those present  
377 on the skin. Wound dressings that can repel or kill bacteria can help obviate the overuse of antibiotics  
378 (Vallet-Regí et al., 2019). Fluorescence images were used to assess the bacteria that were deposited on the  
379 nanofibers. The green dye (SYTO9) permeates the bacterial membranes, indicating live bacteria, while the  
380 red dye (propidium iodide), does not permeate live bacteria, only staining the bacteria that have some defect  
381 or failure in their membrane, staining only dead bacteria (Stiefel et al., 2015). Quantifying bacterial  
382 adhesion is preferable over zone-of-inhibition tests on the nanofibers, due to the similarity with the  
383 conditions in a wound bed. The antibacterial effect observed here is not due to the release and diffusion of  
384 an antibacterial agent (measured by the zone-of-inhibition test). Rather, the antimicrobial activity is present  
385 on the fiber surface, making the evaluation of live/dead bacteria on the surface and bacterial morphology  
386 ideal for this material. **Figures 5 and 6** show fluorescence microscopy images and percentage coverage of  
387 live and dead *S. aureus* and *P. aeruginosa*, respectively, on the nanofibers after 6 h and 24 h. *S. aureus* is a  
388 coccal (round) Gram-positive bacterium, with a thick peptidoglycan-rich cell wall. Conversely, *P.*  
389 *aeruginosa* is a Gram-negative, bacillus (rod-shaped), with a complex and thin cell wall. In general, higher  
390 adhesion of *P. aeruginosa* bacteria is observed in all nanofibers, compared to *S. aureus*, which can be  
391 explained by the greater mobility of the bacteria, due to their flagella (Fredua-Agyeman et al., 2018).  
392 Despite the higher adhesion on the nanofibers, after 6 h of growth, almost all the *P. aeruginosa* adhered to  
393 the CMKC-containing nanofibers were stained red, which characterizes dead bacteria. After 24 h, the PVA  
394 nanofibers have a significant increase in the amount of live bacteria for both bacteria types. The CMKC-  
395 containing nanofibers with higher CMKC content have reduced live bacteria compared to the PVA  
396 nanofibers after 24 hours for both types of bacteria. Furthermore, the 50% and 75% CMKC nanofibers have  
397 an increased number of dead bacteria compared to the PVA nanofibers after 24 hours for both bacteria.

398 Therefore, the CMKC-containing nanofibers do not provide a favorable environment for bacteria, even in  
 399 a nutrient-rich broth condition.

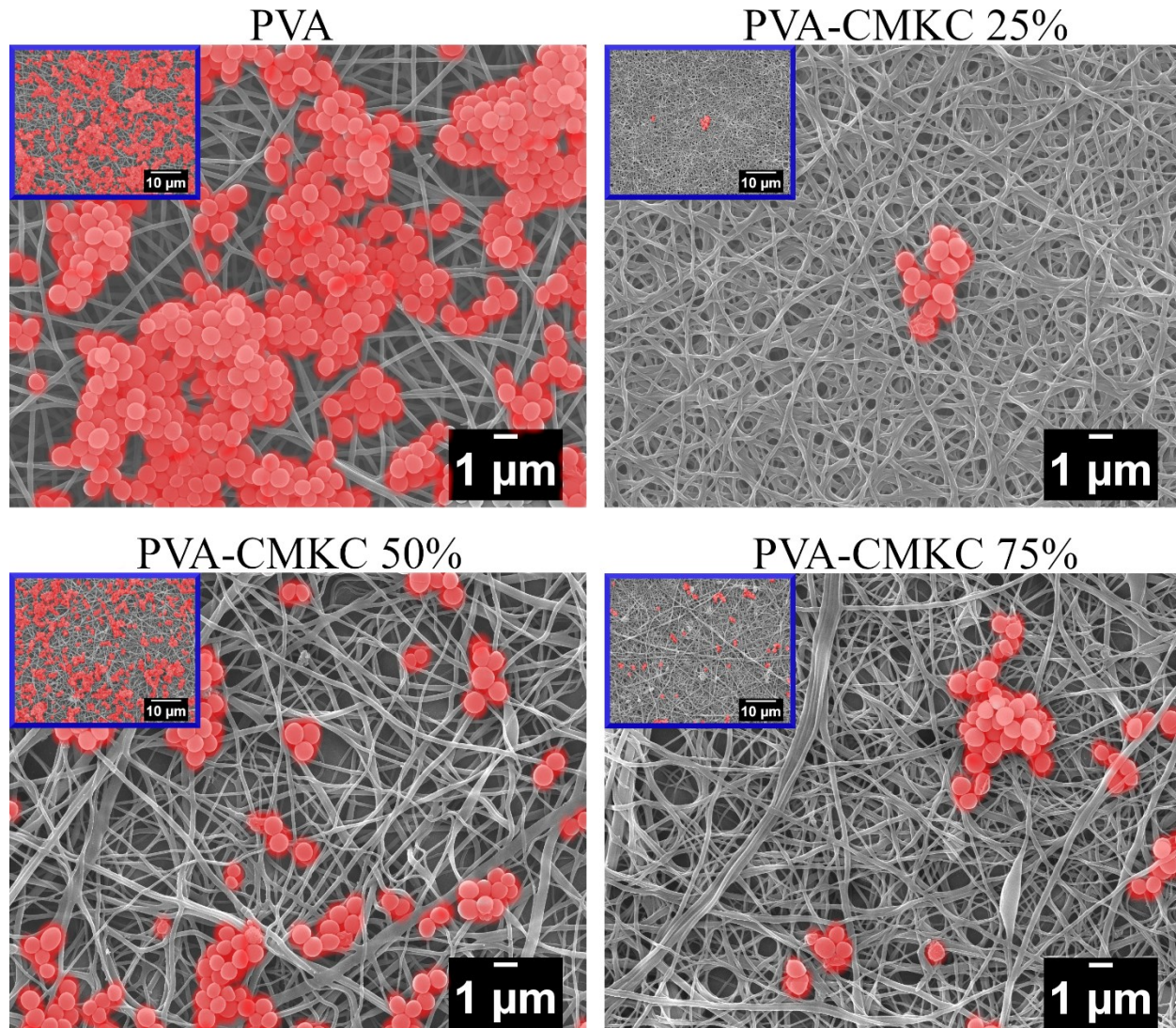


400  
 401 **Figure 5.** Fluorescence microscopy images of *S. aureus* on the nanofibers. Live bacteria are represented  
 402 in green (SYTO 9 stain) and dead bacteria in red (propidium iodide stain) (a). Percentage of coverage for  
 403 live and dead *S. aureus* adhered to the nanofibers. \*\*\*\*  $p \leq 0.0001$ , \*\*\*  $p \leq 0.001$ , \*\*  $p \leq 0.01$ , and "ns"  
 404  $p \geq 0.05$  compared to the PVA control.  
 405

406



421 aggregation. PVA-CMKC nanofibers show a low number of adhered bacteria and few colony formations,  
422 except on 50% CMKC, which may be due to the higher hydrophilicity. Confirming the fluorescence  
423 microscopy data, some bacteria on CMKC-containing fibers have an elliptical shape, and some defective  
424 membranes. These bacteria are probably dead. No biofilm formation was observed on any of the fibers.

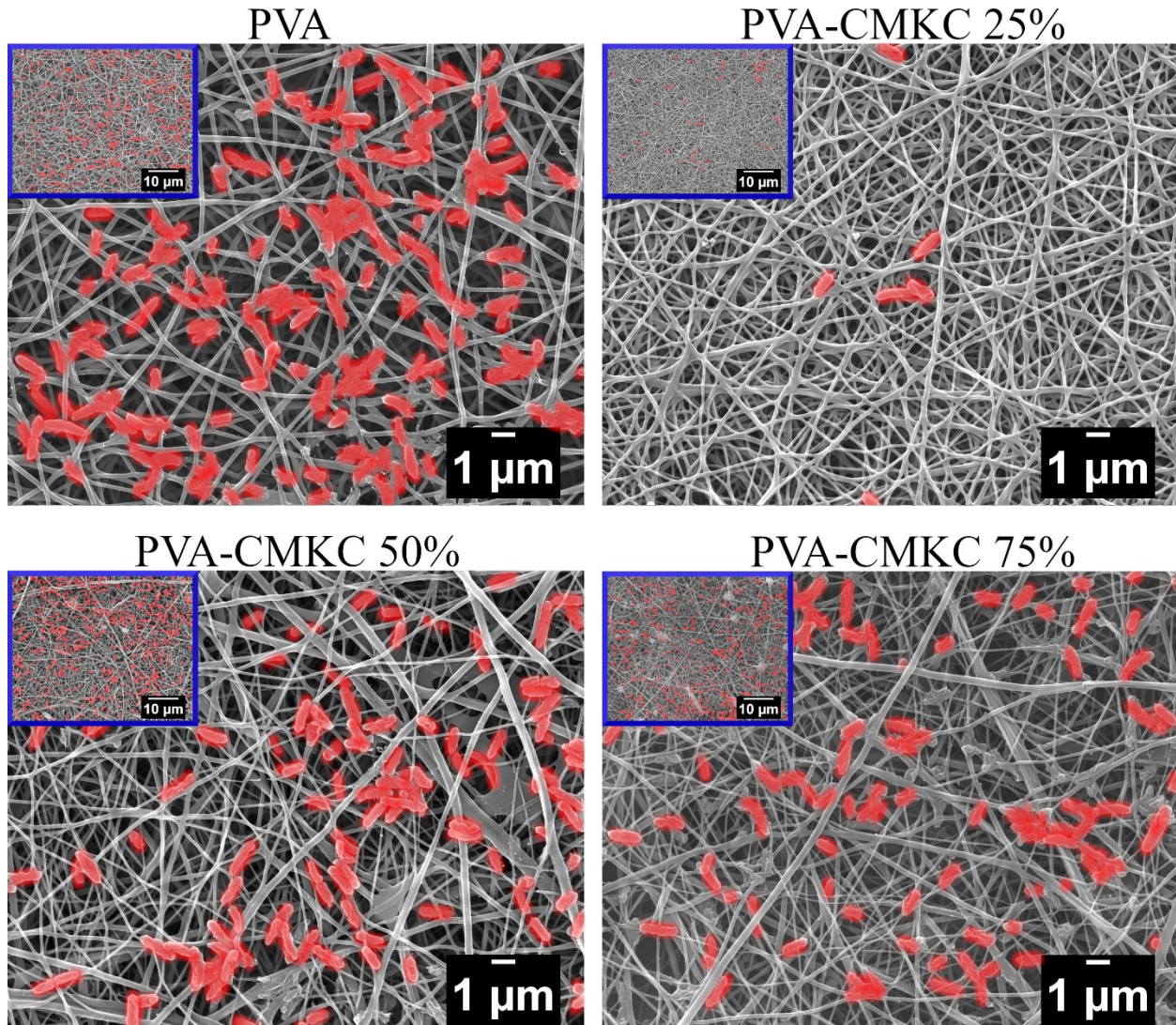


425  
426 **Figure 7.** False colored SEM images of *S. aureus* on the nanofibers after 24 h of incubation.  
427

428 It is important to note that *P. aeruginosa* is a biofilm-forming bacteria, a defense mechanism that  
429 makes it a pathogen that is difficult to fight (Madruga et al., 2020; Reynolds & Neufeld, 2016). After 6 h,  
430 adhered *P. aeruginosa* on the nanofibers (Figure S5 – supplementary information) have a bacillus

431 morphology, and all nanofibers have a high number of bacteria attached. However, some disruptions of the  
432 morphology can be observed, indicating dead bacteria. After 24 h, PVA nanofibers show a higher number  
433 of adhered *P. aeruginosa* (**Figure 8**), as well as colony formation and some biofilm formation. PVA-CMKC  
434 nanofibers also have bacteria attached, but with defective morphology and no biofilm formation,  
435 corroborating the fluorescence microscopy and indicating significant antimicrobial activity.

436 CMKC-containing nanofibers have multiple features that may impart antibacterial activity.  
437 Because they have rigid cell walls, gram-positive and gram-negative bacteria cannot adapt easily to the  
438 nanoscale features, which can lead to cell death on nanostructured surfaces (Vallet-Regí et al., 2019). The  
439 increased hydrophilicity introduced by crosslinking the PVA with CMKC can promote the formation of a  
440 water layer on the surface, generating a physical and energetic barrier for the deposition of bacteria (Wang  
441 et al., 2017). The charged carboxylate and sulfate groups in CMKC can also interact with the bacterial cell  
442 wall and membrane, affecting ion channels and respiratory enzymes, as well as the integrity of the  
443 membrane itself, causing the death of the bacteria (Pajerski et al., 2019).



444

445 **Figure 8.** False colored SEM images of *P. aeruginosa* on the nanofibers after 24 h of incubation.  
446

447 **4. CONCLUSIONS**

448 In this study, electrospun PVA-CMKC nanofibers show enhanced blood coagulation and  
449 antibacterial activity, compared to PVA nanofibers. PVA-CMKC nanofibers preferentially adsorb  
450 fibrinogen compared to albumin, promote platelet adhesion and activation, and promote coagulation in  
451 contact with human whole blood. CMKC-containing nanofibers also exhibit superior antibacterial activity  
452 against both *Staphylococcus aureus* and *Pseudomonas aeruginosa* compared to PVA nanofibers. These  
453 favorable biological properties can be modulated by tuning the CMKC content. These properties are

454 achieved due to a combination of the nanometer-scale features of the fibers and the biologically active  
455 biopolymer containing carboxyl, ether, and sulfate groups. PVA-CMKC nanofibers are non-cytotoxic,  
456 biodegradable, low-cost, and prepared following green manufacturing methods. PVA-CMKC nanofibers  
457 show potential for application as dressings for wound healing applications.

458

459 **ACKNOWLEDGEMENTS**

460 This study was financed in part by the Coordenação de Aperfeiçoamento de Pessoal de Nível  
461 Superior – Brasil (CAPES) – Finance Code 001. Also, the authors gratefully acknowledge the financial  
462 support from the National Science Foundation (award number 1933552).

463

464 **REFERENCES**

465

466 Nas, F. S., Abrigo, M., McArthur, S. L., & Kingshott, P. (2014). Electrospun Nanofibers as Dressings for  
467 Chronic Wound Care: Advances, Challenges, and Future Prospects. *Macromolecular Bioscience*,  
468 14(6), 772–792. <https://doi.org/10.1002/mabi.201300561>

469 Almodóvar, J., Mower, J., Banerjee, A., Sarkar, A. K., Ehrhart, N. P., & Kipper, M. J. (2013). Chitosan-  
470 heparin polyelectrolyte multilayers on cortical bone: Periosteum-mimetic, cytophilic, antibacterial  
471 coatings. *Biotechnology and Bioengineering*, 110(2), 609–618. <https://doi.org/10.1002/bit.24710>

472 Bajpai, S. K., & Daheriya, P. (2014). Kappa-Carrageenan/PVA Films with Antibacterial Properties: Part  
473 1. Optimization of Preparation Conditions and Preliminary Drug Release Studies. *Journal of  
474 Macromolecular Science, Part A*, 51(4), 286–295. <https://doi.org/10.1080/10601325.2014.882687>

475 Barba, B. J. D., Aranilla, C. T., Relleve, L. S., Cruz, V. R. C., Vista, J. R., & Abad, L. V. (2018).  
476 Hemostatic granules and dressing prepared from formulations of carboxymethyl cellulose, kappa-  
477 carrageenan and polyethylene oxide crosslinked by gamma radiation. *Radiation Physics and  
478 Chemistry*, 144(August 2017), 180–188. <https://doi.org/10.1016/j.radphyschem.2017.08.009>

479 Bhattacharjee, A., Clark, R., Gentry-Weeks, C., & Li, Y. V. (2020). A novel receptor-free  
480 polydiacetylene nanofiber biosensor for detecting *E. coli* via colorimetric changes. *Materials  
481 Advances*, 1(9), 3387–3397. <https://doi.org/10.1039/DOMA00619J>

482 Chattopadhyay, S., & Raines, R. T. (2014). Collagen-based biomaterials for wound healing. *Biopolymers*,  
483 101(8), 821–833. <https://doi.org/10.1002/bip.22486>

484 Chiumiento, A., Lamponi, S., & Barbucci, R. (2007). Role of Fibrinogen Conformation in Platelet  
485 Activation. *Biomacromolecules*, 8(2), 523–531. <https://doi.org/10.1021/bm060664m>

486 da Câmara, P. C. F., Madruga, L. Y. C., Sabino, R. M., Vlcek, J., Balaban, R. C., Popat, K. C., Martins,  
487 A. F., & Kipper, M. J. (2020). Polyelectrolyte multilayers containing a tannin derivative polyphenol  
488 improve blood compatibility through interactions with platelets and serum proteins. *Materials  
489 Science and Engineering: C*, 112(March), 110919. <https://doi.org/10.1016/j.msec.2020.110919>

490 da Cruz, J. A., da Silva, A. B., Ramin, B. B. S., Souza, P. R., Popat, K. C., Zola, R. S., Kipper, M. J., &  
491 Martins, A. F. (2020). Poly(vinyl alcohol)/cationic tannin blend films with antioxidant and  
492 antimicrobial activities. *Materials Science and Engineering C*, 107(August 2019), 110357.  
493 <https://doi.org/10.1016/j.msec.2019.110357>

494 Das, A., Abas, M., Biswas, N., Banerjee, P., Ghosh, N., Rawat, A., Khanna, S., Roy, S., & Sen, C. K.  
495 (2019). A Modified Collagen Dressing Induces Transition of Inflammatory to Reparative Phenotype  
496 of Wound Macrophages. *Scientific Reports*, 9(1), 1–10. <https://doi.org/10.1038/s41598-019-49435-z>

497 de Oliveira, M., Madruga, L., de Lima, B., Villetti, M., de Souza Filho, M., Kipper, M., Marques, N., &  
498 Balaban, R. (2021). Agro-Industrial Waste Valorization: Transformation of Starch from Mango  
499 Kernel into Biocompatible, Thermoresponsive and High Swelling Nanogels. *Journal of the*  
500 *Brazilian Chemical Society*, 00(00), 1–10. <https://doi.org/10.21577/0103-5053.20210059>

501 do Nascimento Marques, N., dos Santos Alves, K., Vidal, R. R. L., da Silva Maia, A. M., Madruga, L. Y.  
502 C., Curti, P. S., & de Carvalho Balaban, R. (2020). Chemical Modification of Polysaccharides and  
503 Applications in Strategic Areas. In: F. La Porta & C. Taft (Eds) *Emerging Research in Science and*  
504 *Engineering Based on Advanced Experimental and Computational Strategies. Engineering*  
505 *Materials* (pp. 433–472) Cham: Springer. [https://doi.org/10.1007/978-3-030-31403-3\\_17](https://doi.org/10.1007/978-3-030-31403-3_17)

506 Dorahy, D. J., Thorne, R. F., Fecondo, J. V., & Burns, G. F. (1997). Stimulation of Platelet Activation  
507 and Aggregation by a Carboxyl-terminal Peptide from Thrombospondin Binding to the Integrin-  
508 associated Protein Receptor. *Journal of Biological Chemistry*, 272(2), 1323–1330.  
509 <https://doi.org/10.1074/jbc.272.2.1323>

510 Dumont, M., Villet, R., Guirand, M., Montembault, A., Delair, T., Lack, S., Barikosky, M., Crepet, A.,  
511 Alcouffe, P., Laurent, F., & David, L. (2018). Processing and antibacterial properties of chitosan-  
512 coated alginate fibers. *Carbohydrate Polymers*, 190(December 2016), 31–42.  
513 <https://doi.org/10.1016/j.carbpol.2017.11.088>

514 Fahimirad, S., & Ajalloueian, F. (2019). Naturally-derived electrospun wound dressings for target  
515 delivery of bio-active agents. *International Journal of Pharmaceutics*, 566(May), 307–328.  
516 <https://doi.org/10.1016/j.ijpharm.2019.05.053>

517 Felgueiras, H. P., & Amorim, M. T. P. (2017). Functionalization of electrospun polymeric wound  
518 dressings with antimicrobial peptides. *Colloids and Surfaces B: Biointerfaces*, 156, 133–148.  
519 <https://doi.org/10.1016/j.colsurfb.2017.05.001>

520 Fredua-Agyeman, M., Gaisford, S., & Beezer, A. E. (2018). Observation with microcalorimetry:  
521 Behaviour of *P. aeruginosa* in mixed cultures with *S. aureus* and *E. coli*. *Thermochimica Acta*,  
522 663(March), 93–98. <https://doi.org/10.1016/j.tca.2018.03.009>

523 Fujiwara, T., Nishimoto, S., Ishise, H., Kawai, K., Fukuda, K., & Kakibuchi, M. (2012). Comparative  
524 study of the antibacterial penetrating effects of wound dressings. *Journal of Plastic Surgery and*  
525 *Hand Surgery*, 46(1), 2–7. <https://doi.org/10.3109/2000656X.2011.644939>

526 Guo, J., Zhou, H., Akram, M. Y., Mu, X., Nie, J., & Ma, G. (2016). Characterization and application of  
527 chondroitin sulfate/polyvinyl alcohol nanofibres prepared by electrospinning. *Carbohydrate*  
528 *Polymers*, 143, 239–245. <https://doi.org/10.1016/j.carbpol.2016.02.013>

529 Haider, A., Haider, S., & Kang, I.-K. (2018). A comprehensive review summarizing the effect of  
530 electrospinning parameters and potential applications of nanofibers in biomedical and  
531 biotechnology. *Arabian Journal of Chemistry*, 11(8), 1165–1188.  
532 <https://doi.org/10.1016/j.arabjc.2015.11.015>

533 Hedayati, M., Neufeld, M. J., Reynolds, M. M., & Kipper, M. J. (2019). The quest for blood-compatible  
534 materials: Recent advances and future technologies. *Materials Science and Engineering: R: Reports*,  
535 138(July), 118–152. <https://doi.org/10.1016/j.mser.2019.06.002>

536 Homaeigohar, S., & Boccaccini, A. R. (2020). Antibacterial biohybrid nanofibers for wound dressings.  
537 *Acta Biomaterialia*, 107(2020), 25–49. <https://doi.org/10.1016/j.actbio.2020.02.022>

538 Krauel, K., Hackbarth, C., Fürll, B., & Greinacher, A. (2012). Heparin-induced thrombocytopenia: in  
539 vitro studies on the interaction of dabigatran, rivaroxaban, and low-sulfated heparin, with platelet  
540 factor 4 and anti-PF4/heparin antibodies. *Blood*, 119(5), 1248–1255. <https://doi.org/10.1182/blood-2011-05-353391>

542 Ma, N., Liu, X.-W., Yang, Y.-J., Li, J.-Y., Mohamed, I., Liu, G.-R., & Zhang, J.-Y. (2015). Preventive  
543 Effect of Aspirin Eugenol Ester on Thrombosis in  $\kappa$ -Carrageenan-Induced Rat Tail Thrombosis  
544 Model. *PLOS ONE*, 10(7), e0133125. <https://doi.org/10.1371/journal.pone.0133125>

545 Madruga, L. Y. C., Balaban, R. C., Popat, K. C., & Kipper, M. J. (2021). Biocompatible Crosslinked  
546 Nanofibers of Poly(Vinyl Alcohol)/Carboxymethyl-Kappa-Carrageenan Produced by a Green  
547 Process. *Macromolecular Bioscience*, 21(1), 2000292. <https://doi.org/10.1002/mabi.202000292>

548 Madruga, L. Y. C., da Câmara, P. C. F., Marques, N. do N., & Balaban, R. de C. (2018). Effect of ionic  
549 strength on solution and drilling fluid properties of ionic polysaccharides: A comparative study  
550 between Na-carboxymethylcellulose and Na-kappa-carrageenan responses. *Journal of Molecular  
551 Liquids*, 266, 870–879. <https://doi.org/10.1016/j.molliq.2018.07.016>

552 Madruga, L. Y. C., Sabino, R. M., Santos, E. C. G., Popat, K. C., Balaban, R. de C., & Kipper, M. J.  
553 (2020). Carboxymethyl-kappa-carrageenan: A study of biocompatibility, antioxidant and  
554 antibacterial activities. *International Journal of Biological Macromolecules*, 152, 483–491.  
555 <https://doi.org/10.1016/j.ijbiomac.2020.02.274>

556 Merkle, V. M., Martin, D., Hutchinson, M., Tran, P. L., Behrens, A., Hossainy, S., Sheriff, J., Bluestein,  
557 D., Wu, X., & Slepian, M. J. (2015a). Hemocompatibility of poly(vinyl alcohol)-gelatin core-shell  
558 electrospun nanofibers: A scaffold for modulating platelet deposition and activation. *ACS Applied  
559 Materials and Interfaces*, 7(15), 8302–8312. <https://doi.org/10.1021/acsami.5b01671>

560 Merkle, V. M., Martin, D., Hutchinson, M., Tran, P. L., Behrens, A., Hossainy, S., Sheriff, J., Bluestein,  
561 D., Wu, X., & Slepian, M. J. (2015b). Hemocompatibility of Poly(vinyl alcohol)-Gelatin Core–  
562 Shell Electrospun Nanofibers: A Scaffold for Modulating Platelet Deposition and Activation. *ACS  
563 Applied Materials & Interfaces*, 7(15), 8302–8312. <https://doi.org/10.1021/acsami.5b01671>

564 Miguel, S. P., Figueira, D. R., Simões, D., Ribeiro, M. P., Coutinho, P., Ferreira, P., & Correia, I. J.  
565 (2018). Electrospun polymeric nanofibres as wound dressings: A review. *Colloids and Surfaces B:  
566 Biointerfaces*, 169, 60–71. <https://doi.org/10.1016/j.colsurfb.2018.05.011>

567 Mogoșanu, G. D., & Grumezescu, A. M. (2014). Natural and synthetic polymers for wounds and burns  
568 dressing. *International Journal of Pharmaceutics*, 463(2), 127–136.  
569 <https://doi.org/10.1016/j.ijpharm.2013.12.015>

570 Paar, M., Rossmann, C., Nusshold, C., Wagner, T., Schlagenhauf, A., Leschnik, B., Oettl, K.,  
571 Koestenberger, M., Cvirk, G., & Hallström, S. (2017). Anticoagulant action of low, physiologic, and  
572 high albumin levels in whole blood. *PLoS ONE*, 12(8), 1–12.  
573 <https://doi.org/10.1371/journal.pone.0182997>

574 Pajerski, W., Ochonska, D., Brzychczy-Włoch, M., Indyka, P., Jarosz, M., Golda-Cepa, M., Sojka, Z., &  
575 Kotarba, A. (2019). Attachment efficiency of gold nanoparticles by Gram-positive and Gram-

576 negative bacterial strains governed by surface charges. *Journal of Nanoparticle Research*, 21(8).  
577 <https://doi.org/10.1007/s11051-019-4617-z>

578 Prawel, D. A., Dean, H., Forleo, M., Lewis, N., Gangwish, J., Popat, K. C., Dasi, L. P., & James, S. P.  
579 (2014). Hemocompatibility and Hemodynamics of Novel Hyaluronan–Polyethylene Materials for  
580 Flexible Heart Valve Leaflets. *Cardiovascular Engineering and Technology*, 5(1), 70–81.  
581 <https://doi.org/10.1007/s13239-013-0171-5>

582 Reynolds, B. H. N. M., & Neufeld, B. H. (2016). *Critical nitric oxide concentration for Pseudomonas*  
583 *aeruginosa biofilm reduction on polyurethane substrates*. 031012.  
584 <https://doi.org/10.1116/1.4962266>

585 Rodrigues, S. N., Gonçalves, I. C., Martins, M. C. L., Barbosa, M. A., & Ratner, B. D. (2006). Fibrinogen  
586 adsorption, platelet adhesion and activation on mixed hydroxyl-/methyl-terminated self-assembled  
587 monolayers. *Biomaterials*, 27(31), 5357–5367. <https://doi.org/10.1016/j.biomaterials.2006.06.010>

588 Sabino, R. M., Kauk, K., Madruga, L. Y. C., Kipper, M. J., Martins, A. F., & Popat, K. C. (2020).  
589 Enhanced hemocompatibility and antibacterial activity on titania nanotubes with tanfloc/heparin  
590 polyelectrolyte multilayers. *Journal of Biomedical Materials Research - Part A*, 108(4), 992–1005.  
591 <https://doi.org/10.1002/jbm.a.36876>

592 Sabino, R. M., & Popat, K. C. (2020). Evaluating Whole Blood Clotting in vitro on Biomaterial Surfaces.  
593 *Bio-Protocol*, 10(3), e3505. <https://doi.org/10.21769/BioProtoc.3505>

594 Sabino, R. M., Kauk, K., Movafaghi, S., Kota, A., & Popat, K. C. (2019). Interaction of blood plasma  
595 proteins with superhemophobic titania nanotube surfaces. *Nanomedicine: Nanotechnology, Biology*  
596 *and Medicine*, 21, 102046. <https://doi.org/10.1016/j.nano.2019.102046>

597 Sadeghi, A., Zandi, M., Pezeshki-Modaress, M., & Rajabi, S. (2019). Tough, hybrid chondroitin sulfate  
598 nanofibers as a promising scaffold for skin tissue engineering. *International Journal of Biological*  
599 *Macromolecules*, 132, 63–75. <https://doi.org/10.1016/j.ijbiomac.2019.03.208>

600 Simon-Walker, R., Romero, R., Staver, J. M., Zang, Y., Reynolds, M. M., Popat, K. C., & Kipper, M. J.  
601 (2017). Glycocalyx-Inspired Nitric Oxide-Releasing Surfaces Reduce Platelet Adhesion and  
602 Activation on Titanium. *ACS Biomaterials Science & Engineering*, 3(1), 68–77.  
603 <https://doi.org/10.1021/acsbiomaterials.6b00572>

604 Sivaraman, B., & Latour, R. A. (2010). The relationship between platelet adhesion on surfaces and the  
605 structure versus the amount of adsorbed fibrinogen. *Biomaterials*, 31(5), 832–839.  
606 <https://doi.org/10.1016/j.biomaterials.2009.10.008>

607 Stiefel, P., Schmidt-Emrich, S., Maniura-Weber, K., & Ren, Q. (2015). Critical aspects of using bacterial  
608 cell viability assays with the fluorophores SYTO9 and propidium iodide. *BMC Microbiology*, 15(1),  
609 36. <https://doi.org/10.1186/s12866-015-0376-x>

610 Tranquilan-Aranilla, C., Barba, B. J. D., Vista, J. R. M., & Abad, L. V. (2016). Hemostatic efficacy  
611 evaluation of radiation crosslinked carboxymethyl kappa-carrageenan and chitosan with varying  
612 degrees of substitution. *Radiation Physics and Chemistry*, 124, 124–129.  
613 <https://doi.org/10.1016/j.radphyschem.2016.02.003>

614 Trinca, R. B., Westin, C. B., da Silva, J. A. F., & Moraes, Â. M. (2017). Electrospun multilayer chitosan  
615 scaffolds as potential wound dressings for skin lesions. *European Polymer Journal*, 88, 161–170.  
616 <https://doi.org/10.1016/j.eurpolymj.2017.01.021>

617 Truong, Y. B., Glattauer, V., Briggs, K. L., Zappe, S., & Ramshaw, J. A. M. (2012). Collagen-based  
618 layer-by-layer coating on electrospun polymer scaffolds. *Biomaterials*, 33(36), 9198–9204.

619 http://dx.doi.org/10.1016/j.biomaterials.2012.09.012

620 Unnithan, A. R., Sasikala, A. R. K., Murugesan, P., Gurusamy, M., Wu, D., Park, C. H., & Kim, C. S.  
621 (2015). Electrospun polyurethane-dextran nanofiber mats loaded with Estradiol for post-menopausal  
622 wound dressing. *International Journal of Biological Macromolecules*, 77, 1–8.  
623 https://doi.org/10.1016/j.ijbiomac.2015.02.044

624 Vallet-Regí, M., González, B., & Izquierdo-Barba, I. (2019). Nanomaterials as promising alternative in  
625 the infection treatment. *International Journal of Molecular Sciences*, 20(15).  
626 https://doi.org/10.3390/ijms20153806

627 Vlcek, J. R., Hedayati, M., Melvin, A. C., Reynolds, M. M., & Kipper, M. J. (2021). Blood-Compatible  
628 Materials: Vascular Endothelium-Mimetic Surfaces that Mitigate Multiple Cell-Material  
629 Interactions. *Advanced Healthcare Materials*, 10(7), 2001748.  
630 https://doi.org/10.1002/adhm.202001748

631 Vögtle, T., Sharma, S., Mori, J., Nagy, Z., Semeniak, D., Scandola, C., Geer, M. J., Smith, C. W., Lane,  
632 J., Pollack, S., Lassila, R., Jouppila, A., Barr, A. J., Ogg, D. J., Howard, T. D., McMiken, H. J.,  
633 Warwicker, J., Geh, C., Rowlinson, R., ... Senis, Y. A. (2019). Heparan sulfates are critical  
634 regulators of the inhibitory megakaryocyte-platelet receptor G6b-B. *ELife*, 8, 1–43.  
635 https://doi.org/10.7554/eLife.46840

636 Wang, L., Hu, C., & Shao, L. (2017). The-antimicrobial-activity-of-nanoparticles--present-situati.  
637 *International Journal of Nanomedicine*, 12, 1227–1249. https://doi.org/10.2147/IJN.S121956

638 Wilner, G. D., Nossel, H. L., & LeRoy, E. C. (1968). Aggregation of platelets by collagen. *Journal of*  
639 *Clinical Investigation*, 47(12), 2616–2621. https://doi.org/10.1172/JCI105944

640 Xu, F., Weng, B., Gilkerson, R., Materon, L. A., & Lozano, K. (2015). Development of tannic  
641 acid/chitosan/pullulan composite nanofibers from aqueous solution for potential applications as  
642 wound dressing. *Carbohydrate Polymers*, 115, 16–24. https://doi.org/10.1016/j.carbpol.2014.08.081

643 Yang, L., Han, L., Liu, Q., Xu, Y., & Jia, L. (2017). Galloyl groups-regulated fibrinogen conformation:  
644 Understanding antiplatelet adhesion on tannic acid coating. *Acta Biomaterialia*, 64, 187–199.  
645 https://doi.org/10.1016/j.actbio.2017.09.034

646 Yegappan, R., Selvapritchivraj, V., Amirthalingam, S., & Jayakumar, R. (2018). Carrageenan based  
647 hydrogels for drug delivery, tissue engineering and wound healing. *Carbohydrate Polymers*,  
648 198(June), 385–400. https://doi.org/10.1016/j.carbpol.2018.06.086

649 Young, B. M., Shankar, K., Allen, B. P., Pouliot, R. A., Schneck, M. B., Mikhail, N. S., & Heise, R. L.  
650 (2017). Electrospun Decellularized Lung Matrix Scaffold for Airway Smooth Muscle Culture. *ACS*  
651 *Biomaterials Science & Engineering*, 3(12), 3480–3492.  
652 https://doi.org/10.1021/acsbiomaterials.7b00384

653 Zahedi, P., Rezaeian, I., Ranaei-Siadat, S.-O., Jafari, S.-H., & Supaphol, P. (2010). A review on wound  
654 dressings with an emphasis on electrospun nanofibrous polymeric bandages. *Polymers for Advanced*  
655 *Technologies*, 21(2), 77–95. https://doi.org/10.1002/pat.1625

656 Zeng, Q., Qin, J., Yin, X., Liu, H., Zhu, L., Dong, W., & Zhang, S. (2016). Preparation and  
657 hemocompatibility of electrospun O-carboxymethyl chitosan/PVA nanofibers. *Journal of Applied*  
658 *Polymer Science*, 133(26), 2–9. https://doi.org/10.1002/app.43565

659 Zhang, L., Casey, B., Galanakis, D. K., Marmorat, C., Skoog, S., Vorvolakos, K., Simon, M., &  
660 Rafailovich, M. H. (2017). The influence of surface chemistry on adsorbed fibrinogen conformation,  
661 orientation, fiber formation and platelet adhesion. *Acta Biomaterialia*, 54, 164–174.

662 <https://doi.org/10.1016/j.actbio.2017.03.002>

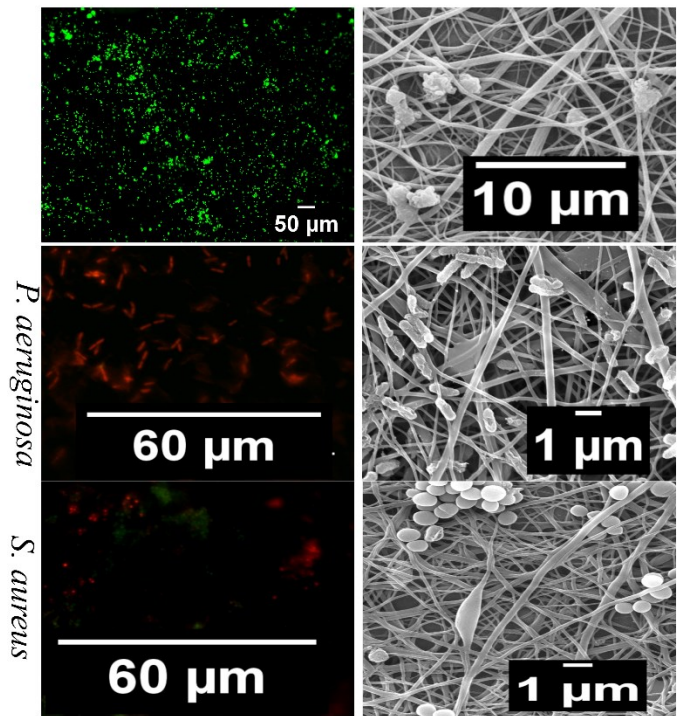
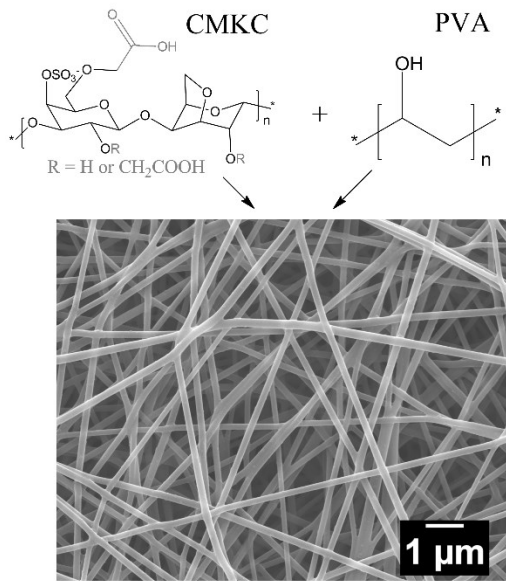
663 Zhao, R., Li, X., Sun, B., Zhang, Y., Zhang, D., Tang, Z., Chen, X., & Wang, C. (2014). Electrospun  
664 chitosan/sericin composite nanofibers with antibacterial property as potential wound dressings.  
665 *International Journal of Biological Macromolecules*, 68, 92–97.  
666 <https://doi.org/10.1016/j.ijbiomac.2014.04.029>

667 Zhao, X., Gao, J., Hu, X., Guo, H., Wang, F., Qiao, Y., & Wang, L. (2018). Collagen/Polyethylene Oxide  
668 Nanofibrous Membranes with Improved Hemostasis and Cytocompatibility for Wound Dressing.  
669 *Applied Sciences*, 8(8), 1226. <https://doi.org/10.3390/app8081226>

670 Zia, K. M., Tabasum, S., Nasif, M., Sultan, N., Aslam, N., Noreen, A., & Zuber, M. (2017). A review on  
671 synthesis, properties and applications of natural polymer based carrageenan blends and composites.  
672 *International Journal of Biological Macromolecules*, 96, 282–301.  
673 <https://doi.org/10.1016/j.ijbiomac.2016.11.095>

674

## Blood coagulation



## Antibacterial activity